Journal of Power Sources 230 (2013) 59–65

Contents lists available at SciVerse ScienceDirect

Journal of Power Sources

journal homepage: www.elsevier.com/locate/jpowsour

Synthesis and electrochemical properties of sticktight-like and nanosheet Co_3O_4 particles

X.Y. Feng [a], C. Shen [a], Y. Yu [a], S.Q. Wei [b], C.H. Chen [a,*]

[a] CAS Key Laboratory of Materials for Energy Conversions, Department of Materials Science and Engineering, University of Science and Technology of China, Anhui, Hefei 230026, China
[b] National Laboratory of Synchrotron Radiation, Anhui, Hefei 230026, China

HIGHLIGHTS

- Sticktight-like and nanosheet-like Co_3O_4 particles are prepared by a hydrothermal reaction and subsequent calcination.
- Nanosheet-like Co_3O_4 shows better rate capability than sticktight Co_3O_4.
- A relatively low initial capacity loss (16%) can be achieved.

ARTICLE INFO

Article history:
Received 17 September 2012
Received in revised form
20 November 2012
Accepted 11 December 2012
Available online 20 December 2012

Keywords:
Lithium battery
Cobalt oxide
Nanostructure
Thermogravimetry
X-ray absorption fine structure spectroscopy

ABSTRACT

Sticktight-like particles and nanosheets of basic cobaltous carbonates of different morphologies are synthesized through a hydrothermal process. Their structures and formulas are characterized by X-ray diffraction, scanning electron microscopy, transmission electron microscopy, X-ray absorption fine structure and thermogravimetry. After being calcined at 400 °C and 500 °C, these basic cobaltous carbonates change into Co_3O_4 powders and are used as electrode materials of lithium ion batteries. The electrochemical test shows that Co_3O_4 powders with different morphologies are of different electrochemical performance. Owing to the better mechanical strength and better continuity for electron conduction compared with the sticktight-like Co_3O_4 samples, the 400 °C- and 500 °C-calcined nanosheet Co_3O_4 samples show better cycling performance and rate performance. They retain a capacity of over 700 mAh g^{-1} at 10 C current density. The 400 °C-calcined nanosheet Co_3O_4 sample exhibits a low initial capacity loss of 18.8%. An even less initial capacity loss of about 15.6% is measured for the sticktight-like Co_3O_4 sample.

1. Introduction

Lithium ion batteries with graphite as the anode and $LiCoO_2$ as the cathode active materials have achieved huge success in the field of portable electronic devices. Graphite has a reasonably high theoretical capacity of 372 mAh g^{-1} and good cycle performance which can satisfy the needs of small electronic appliance such as mobile phones. However, the specific capacity of the graphite is still too low for electric vehicles. On the other hand, the high discharge–charge rate performance is important in the design and development of electrode materials that meet the requirement of advanced Li-ion batteries for electrical vehicles but the electrochemical performance of graphite at high rate current density is actually quite poor. In the past decade, many efforts have been made to search for alternative materials with higher specific capacity and better rate performance. Transition metal oxides, especially like cobalt oxides (CoO [1–3], Co_3O_4 [4–6]) have been proposed as alternative anode materials due to their high Li-storage capacities. However, the cycling performances and rate performance of the bulk cobalt oxides are very poor due to the huge volume change during the charge–discharge processes and low conductivity. Cobalt oxides with nanostructures have high specific surface and short lithium diffusion distance, which is beneficial for the specific capacity and rate performance. On the other hand, the nanostructures of cobalt oxides can sustain more volume change during the electrochemical cycling process. In the past decades, cobalt oxides of different nanostructures including nanotubes [7–9], nanowires [10–12], nanobelts [13,14], nanoneedles [15] and films [16–19] have been prepared. These efforts have resulted in better electrochemical performances of cobalt oxides.

* Corresponding author. Tel.: +86 551 3606971; fax: +86 551 3601952.
E-mail address: cchchen@ustc.edu.cn (C.H. Chen).

0378-7753/$ – see front matter © 2012 Elsevier B.V. All rights reserved.
http://dx.doi.org/10.1016/j.jpowsour.2012.12.046

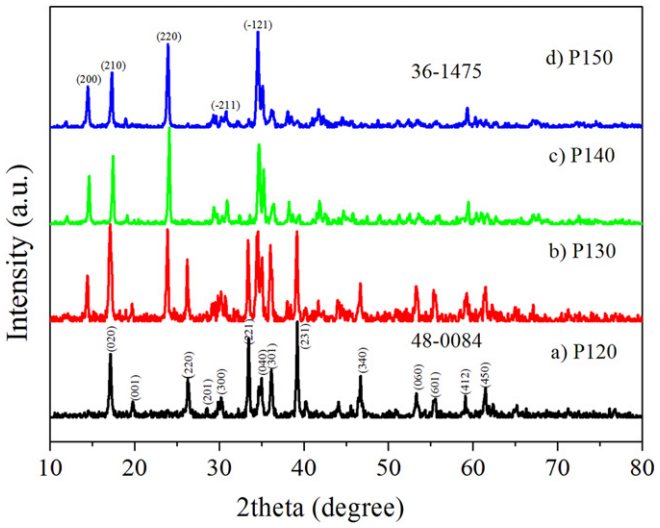

Fig. 1. XRD patterns of cobalt precipitations at 120 °C (a), 130 °C (b), 140 °C (c) and 150 °C (d).

In this study, basic cobaltous carbonates of one-dimensional (sticktight-like) and two-dimensional (nanosheet) structures have been synthesized by a hydrothermal process. Although their derived Co_3O_4 samples have the similar high capacity and good cycling performance, the rate performance of the nanosheet sample is better for its better mechanical strength.

2. Experimental

Basic cobaltous carbonate powders of sticktight-like particles and nanosheets were synthesized through a hydrothermal process. 0.2911 g cobalt nitrate ($Co(NO_3)_2 \cdot 4H_2O$, 1 mmol), 0.06 g urea ($CO(NH_2)_2$, 1 mmol) and 0.05 g resorcinol ($C_6H_4(OH)_2$) were dissolved in 40 ml distilled water. Then the solution was transferred to a Teflon lined autoclave (50 ml) and placed in an electric oven heated at different temperatures (120, 130, 140 and 150 °C) for about 20 h. After the hydrothermal process, some pink powders were separated out of the solution. These powders were washed by water and alcohol for several times and then dried in a vacuum oven at 70 °C. These samples were named as P120, P130, P140 and P150, corresponding to their different hydrothermal temperatures 120, 130, 140 and 150 °C, respectively. Then the particles with uniform morphology (P120, P150) were calcined at 400 or 500 °C for 5 h to obtain cobalt oxides. As a comparison, a commercial $CoCO_3$ was also calcined at 400 °C to obtain cobalt (II, III) oxide (Co_3O_4).

The crystalline structures of the powders obtained at different temperatures and calcined cobalt oxides were characterized by X-ray diffraction (XRD) using a diffractometer (Rigaku, Cu Kα radiation). The diffraction patterns were recorded at room temperature in the 2θ range from 10° to 80°. The morphology and particle size were characterized by scanning electron microscopy (SEM, JSM-6390LA, JEOL) and transmission electron microscopy (TEM, Hitachi H-800). X-ray absorption fine structure spectroscopy (XAFS) of the powders was performed in the National Laboratory of Synchrotron Radiation (NLSR, Hefei, China) with a ring energy of 0.8 GeV, and a current of 250 mA. Thermogravimetry (TG) was performed using a Shimadzu DT 50 thermal analyzer with a heating rate of 10 °C min^{-1} in air.

The electrochemical properties of Co_3O_4 samples were measured in the CR2032 coin-type half-cells Co_3O_4/Li using 1 M LiPF6 in EC: DEC (1:1 v/v) as the electrolyte. The positive electrodes consisted of a mixture of Co_3O_4 samples, acetylene black and PVDF binder in the weight ratio of 40:30:30. The cells were assembled in an argon-filled dry-box (MBraun Labmaster 130) with a porous polypropylene membrane (Celgard 2400) as the separator. They were cycled on a multi-channel battery test system (NEWARE BTS-610) in the constant current charge–discharge mode in the voltage range from 0.01 V to 3.0 V.

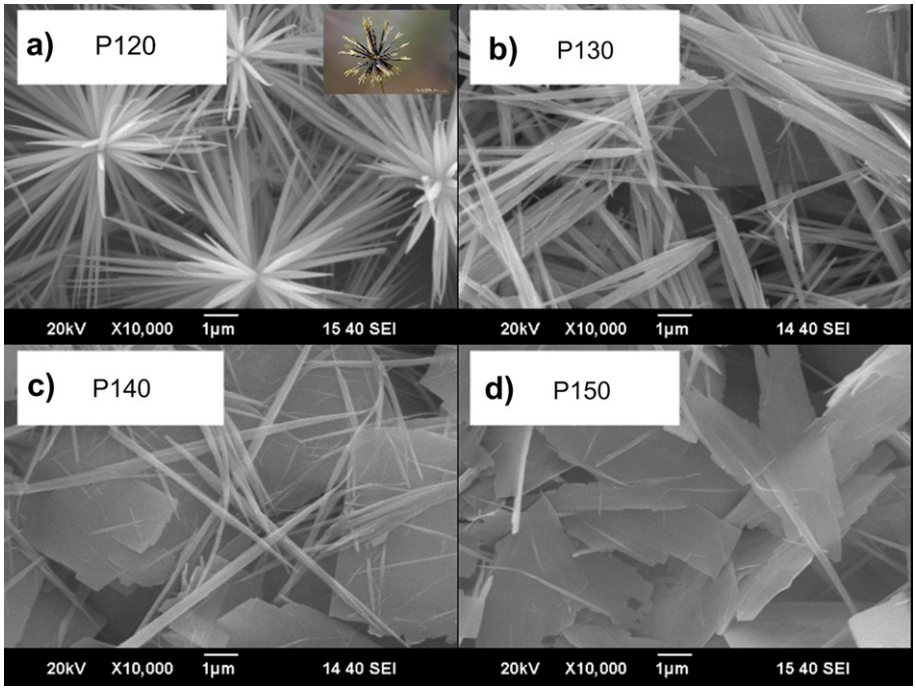

Fig. 2. SEM images of cobalt precipitates at 120 °C (a), 130 °C (b), 140 °C (c) and 150 °C (d).

3. Results and discussion

3.1. Structure and morphology

The XRD patterns of P120, P130, P140 and P150 are shown in Fig. 1. The sample of P120 can be indexed to the phase of $Co(OH)_{1.3}(CO_3)_{0.35}\cdot xH_2O$ (JPCPDF 38-0547) or $Co(OH)_{1.14}(CO_3)_{0.43}$ (JPCPDF 48-0048, P2212). Note that, the ratio of CO_3^{2-} and OH^- cannot be determined by such a simple XRD analysis. When the hydrothermal temperature increases, other peaks at about 14°, 24° and 34° become stronger while the peaks at 26°, 33° and 39° become weaker. When the temperature increases to 150 °C, the orthorhombic phase ($P22_12$) almost disappears and another monoclinic phase become the major phase (JPCPDF 36-1475, $P2_1/a$, $Co(CO_3)_{0.5}OH$). It is another kind of basic cobaltous carbonate with a different molar ratio between CO_3^{2-} and OH^-. The XRD pattern of P150 fits the standard cards well but the second strongest peak at about 30° (lattice plane (−211)) is quite weak, which means the crystal may grow along the surface of (−211) and to form thin plates.

The SEM images of P120 to P150 are shown in Fig. 2. It can be seen that the particle morphology is highly impacted by the hydrothermal temperature, changing from a sticktight-like morphology for P120 to a nanosheet for P150. The sticktight-like particles are comprised of nanoneedles of tens of nanometers in diameter and tens of micrometers in length (Fig. 2a, P120). With increasing the temperature, a growing number of nanosheet particles are generated (Fig. 2b, c). When the temperature rises up to 150 °C, the morphology of the product is almost all nanosheets (Fig. 2d). Since P120 and P150 are of different structures (orthorhombic for sticktight-like particles and monoclinic for nanosheets), it means different structures have different preferential orientations and lead to 1D or 2D nanostructure. The TEM images and SAED patterns of P120 and P150 of uniform morphology are shown in Fig. 3. The SAED patterns show different lattice structures and high crystallinity of these two samples with different morphologies.

Although both P120 and P150 are basic cobaltous carbonate according to above XRD analysis, their real chemical formulas are not very clear. Thus, they are further characterized by XAFS test and TG analyses. XAFS (Fig. 4) is used to characterize the valence state of cobalt and the groups around the cobalt atom. It is seen in Fig. 4 that both the sticktight-like sample (P120) and the nanosheet sample (P150) show an XAFS spectrum similar to that of the commercial $CoCO_3$. Their main absorption peaks are all located at about 7727 eV, suggesting that the valence state of cobalt in these products is all divalent (+2). The differences in the intensities and positions for other peaks may imply that they have different coordination structures by either CO_3^{2-} or both CO_3^{2-} and OH^- groups.

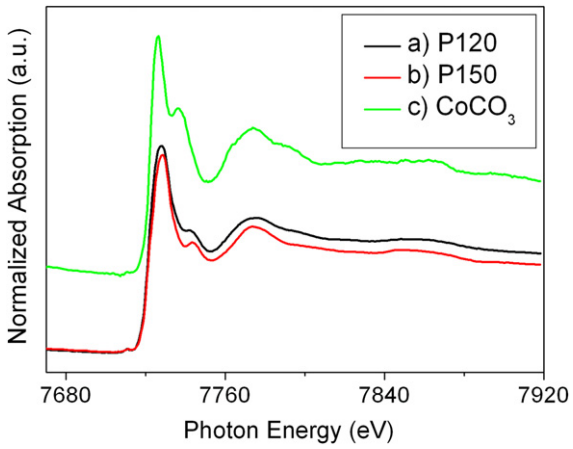

Fig. 4. XAFS spectra of cobalt precipitates synthesized at 120 °C (a), 150 °C (b) and commercial $CoCO_3$.

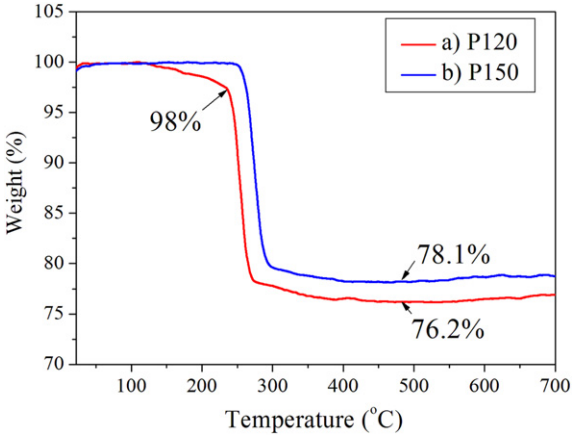

Fig. 5. TG curves of cobalt precipitates obtained at 120 °C (a) and 150 °C (b).

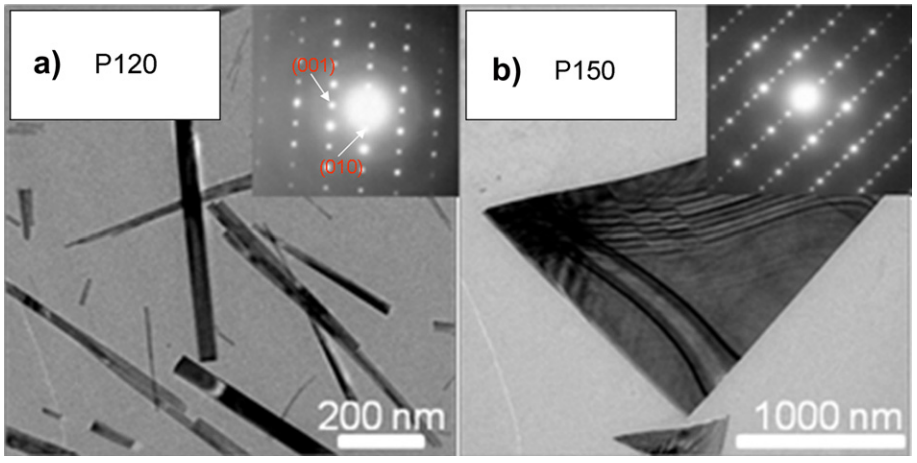

Fig. 3. TEM image and SAED pattern of cobalt precipitates at 120 °C (a) and 150 °C (b).

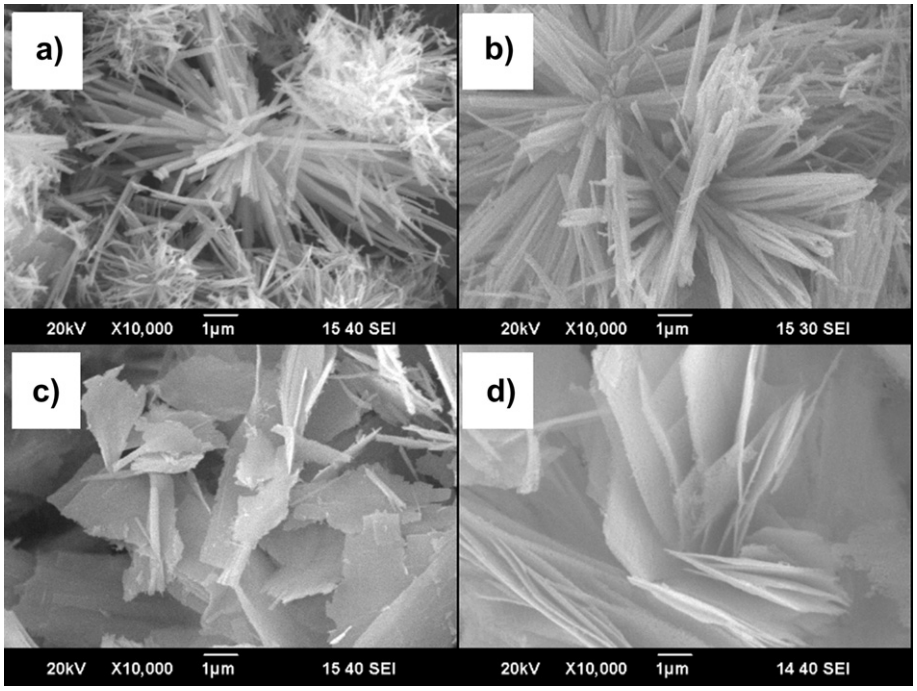

Fig. 6. SEM micrographs of: a) sticktight-like Co_3O_4 calcined at 400 °C; b) sticktight-like Co_3O_4 calcined at 500 °C; c) nanosheet Co_3O_4 calcined at 400 °C; and d) nanosheet Co_3O_4 calcined at 500 °C.

The TG curves of P120 and P150 are shown in Fig. 5. A major weight loss process at about 250 °C is observed for both samples due probably to the decompositions of hydroxyl and carbonate groups. Nevertheless, an additional small weight loss process from 150 to 250 °C is observed for P120, which can be attributed to the loss of the crystal water. Because the final products of these TG analyses are determined to be Co_3O_4 (see below for the XRD results, Fig. 7), the formulas of P120 and P150 can be calculated to be $Co(OH)_{1.3}(CO_3)_{0.35}\cdot 0.14H_2O$ and $Co(OH)_{1.24}(CO_3)_{0.38}$, respectively, after considering the quantitative results of the weight losses. Apparently, the minor change in the ratio between OH^- and CO_3^{2-} leads to a substantial change in the particle morphology.

After being calcined at 400 °C or 500 °C, all of the basic cobaltous carbonates are expected to become cobalt oxides. Fig. 6 shows

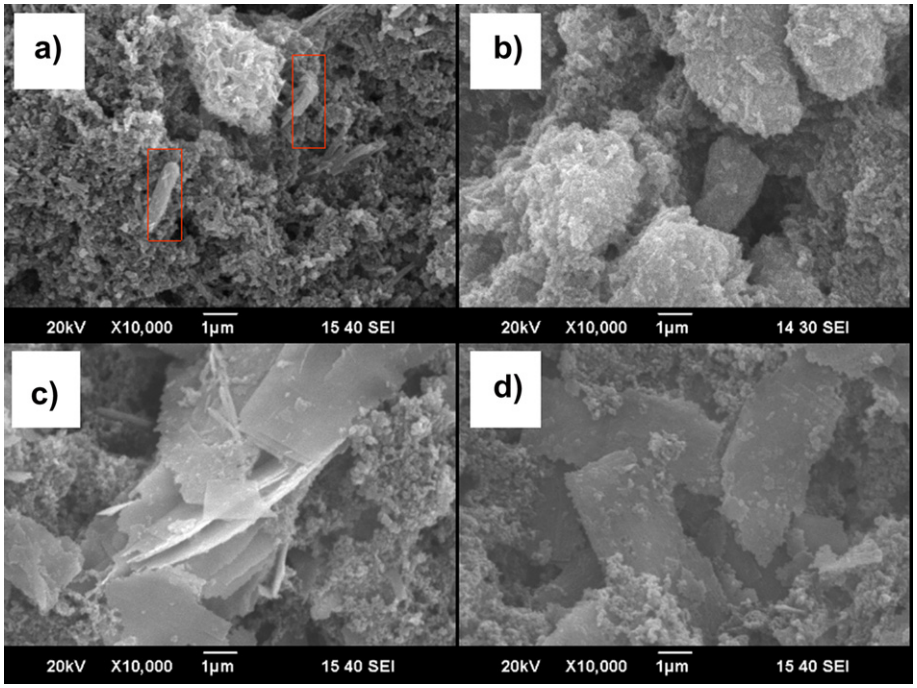

Fig. 7. SEM micrographs of the electrode laminates made of different Co_3O_4 particles: a) sticktight-like Co_3O_4 calcined at 400 °C; b) sticktight-like Co_3O_4 calcined at 500 °C; c) nanosheet Co_3O_4 calcined at 400 °C and d) nanosheet Co_3O_4 calcined at 500 °C.

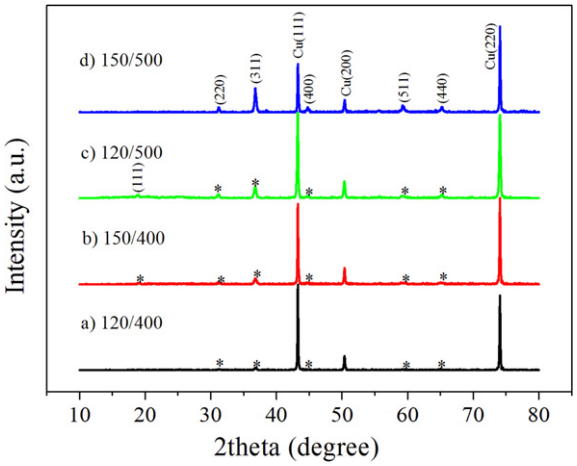

Fig. 8. XRD patterns of the prepared Co_3O_4: a) sticktight-like Co_3O_4 calcined at 400 °C; b) sticktight-like Co_3O_4 calcined at 500 °C; c) nanosheet Co_3O_4 calcined at 400 °C and d) nanosheet Co_3O_4 calcined at 500 °C.

that nanostructures of sticktights and nanosheets can retain after the calcination. However, after a grinding during the preparation of electrode laminates, the sticktight-like morphology is broken into smaller particles (Fig. 7a, b) while the nanosheet morphology can still be largely retained (Fig. 7c, d). Furthermore, the samples calcined at 400 °C (Fig. 7a, c) are more stable than those calcined at 500 °C (Fig. 7b, d), because some short needle-like particles can be found in P120 after being calcined at 400 °C (Fig. 7a, the framed particles) but have disappeared after being calcined at 500 °C (Fig. 7b). Also, more intact nanosheets are observed in P150 after being calcined at 400 °C (Fig. 7c) than after being calcined at 500 °C (Fig. 7d). The XRD patterns of the calcined products on a copper foil (Fig. 8) indicate that except for the diffraction peaks from the copper substrate they all belong to a pure-phase of Co_3O_4 with different degrees of crystallinity depending on the calcination temperature. Because the diffraction peaks of these samples calcined at 400 °C are very weak, we do not calcine the samples at a lower temperature.

3.2. Electrochemical performance of Co_3O_4

Transition metal oxides always have a high specific capacity of about hundreds of milliamperes per gram. All of the cobalt oxides obtained through different routines have high capacities. It can be seen in Fig. 9 that the sticktight-like structure oxide shows a high specific capacity of over 1000 mAh g^{-1} at the second cycle (Fig. 9a, b), which is higher than those of the nanosheet-Co_3O_4 electrodes (Fig. 9c, d). This higher capacity may be attributed to their higher specific surface because the sticktight-like samples have broken into nanoparticles during the electrode preparation process. The specific capacity of the nanosheet samples is somewhat lower but it is still as high as 900 mAh g^{-1}. There are two plateaus at about 1.1 V and 1.0 V, respectively, on the first discharge curve which are generally attributed to the partial reduction process into $Li_xCo_3O_4$ [20] and the reduction into metallic cobalt. Note that, the high voltage plateau at 1.1 V is only observed for the nanostructured Co_3O_4 with high specific surface area. The sloping curve from 1.0 V to 0.01 V should be mainly related to the reversible interface lithium storage [21] or the formation of a gel-like film [22,23], which results in the higher capacity than the theoretical capacity calculated based on the traditional theory ($Co_3O_4 + 8Li = 3Co + 4Li_2O$, 890 mAh g^{-1}). Also, to a small extent, the formation of a so-called solid electrolyte interphase (SEI) layer occurs in this discharge process. Note that the formation of SEI layer is irreversible and leads to some initial capacity loss. The samples calcined at 400 °C show a low initial capacity loss of 15.6% for the sticktight-like sample (Fig. 9a) and 18.8% for the nanosheet sample (Fig. 9c),

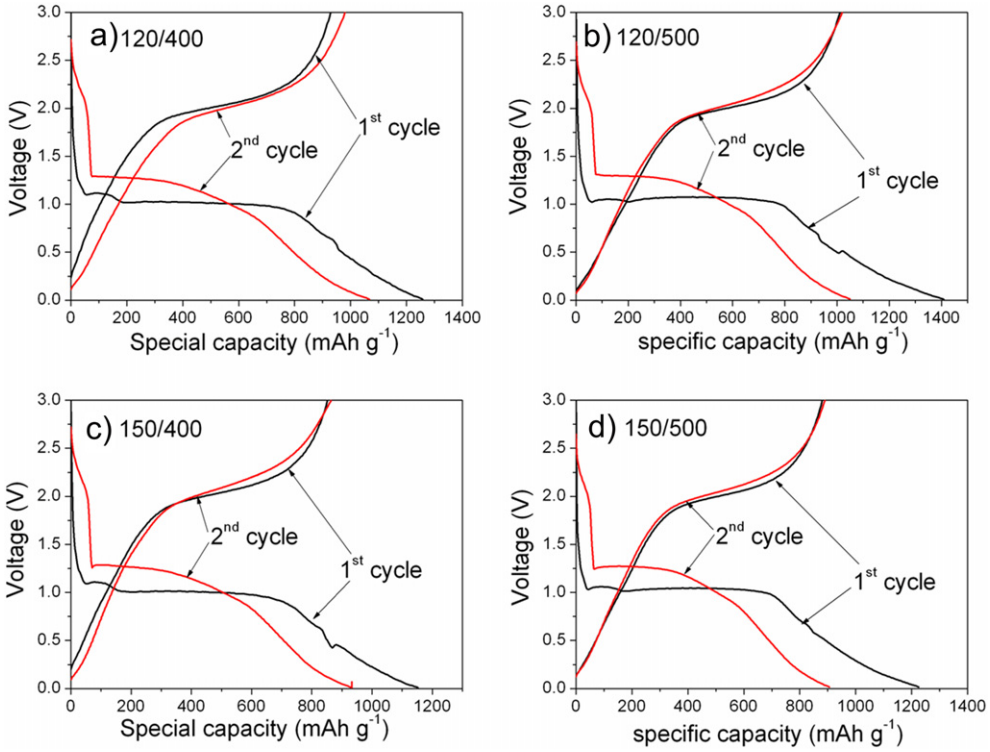

Fig. 9. Voltage profiles of different Co_3O_4 samples: a) sticktight-like Co_3O_4 calcined at 400 °C; b) sticktight-like Co_3O_4 calcined at 500 °C; c) nanosheet Co_3O_4 calcined at 400 °C and d) nanosheet Co_3O_4 calcined at 500 °C. The electrode composition is Co_3O_4:AB:PVDF = 40:30:30 and measured at a current density of 300 mA g^{-1}.

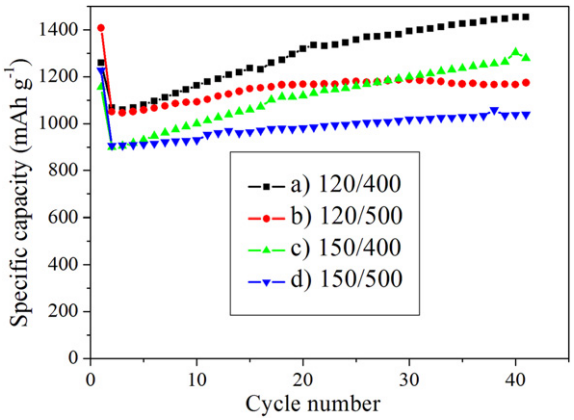

Fig. 10. Cycle performance of different Co_3O_4 samples: a) sticktight-like Co_3O_4 calcined at 400 °C; b) sticktight-like Co_3O_4 calcined at 500 °C; c) nanosheet Co_3O_4 calcined at 400 °C and d) nanosheet Co_3O_4 calcined at 500 °C.

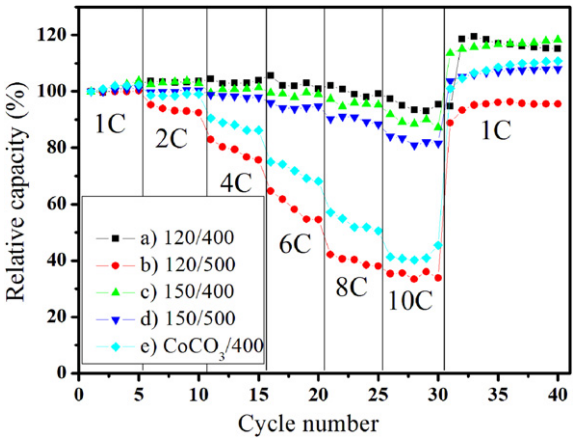

Fig. 12. Rate performance of different Co_3O_4 samples: a) sticktight-like Co_3O_4 calcined at 400 °C; b) sticktight-like Co_3O_4 calcined at 500 °C; c) nanosheet Co_3O_4 calcined at 400 °C; d) nanosheet Co_3O_4 calcined at 500 °C and commercial $CoCO_3$ calcined at 400 °C.

which is quite low among the transition metal oxide anodes. The low initial capacity loss is very important and desirable to the anode materials because the corresponding irreversible reactions consume active lithium form the cathode side and a high initial capacity loss would lead to a low capacity of the full cell. Usually, transition metal oxides have a higher initial capacity loss than graphite because not all of the electrochemical reactions during the first discharge process are reversible. The initial capacity loss of most oxides is as high as 30% or even more [24–27], which has limited the application of oxide-based anodes.

The cycling performances of these materials are shown in Fig. 10. The capacities of these samples increase after the second cycle and even surpass the initial capacity after several cycles (Fig. 10a, c). The increase of capacity can be attributed to the pulverization of the cobalt oxides that leads to increasing surface area. After about 40 cycles, the specific capacities become stable and the highest capacity can reach 1450 mAh g^{-1} (Fig. 10a, the sticktight-like sample after being calcined at 400 °C). Also, most of these samples can retain a specific capacity of over 900 mAh g^{-1}, which is much higher than that of graphite (372 mAh g^{-1}). After 40 cycles and disassembling the cell, it is found that the short nanoneedle cobalt oxide in the electrode has been pulverized to smaller particles (Fig. 11) and no short nanoneedle particles can be found any more. For comparison, the nanosheet sample is more stable so that the morphology retains to a large extent even after 40 cycles (Fig. 11c, d).

Fig. 12 shows the rate capabilities of these samples. The rate performances of both the sticktight-like and nanosheet samples after being calcined at 400 °C are quite good with a capacity of over 800 mAh g^{-1} retained at the rate of 10 C, which are a little less than that at the rate of 1 C (Fig. 12a, c). The capacities also increase during

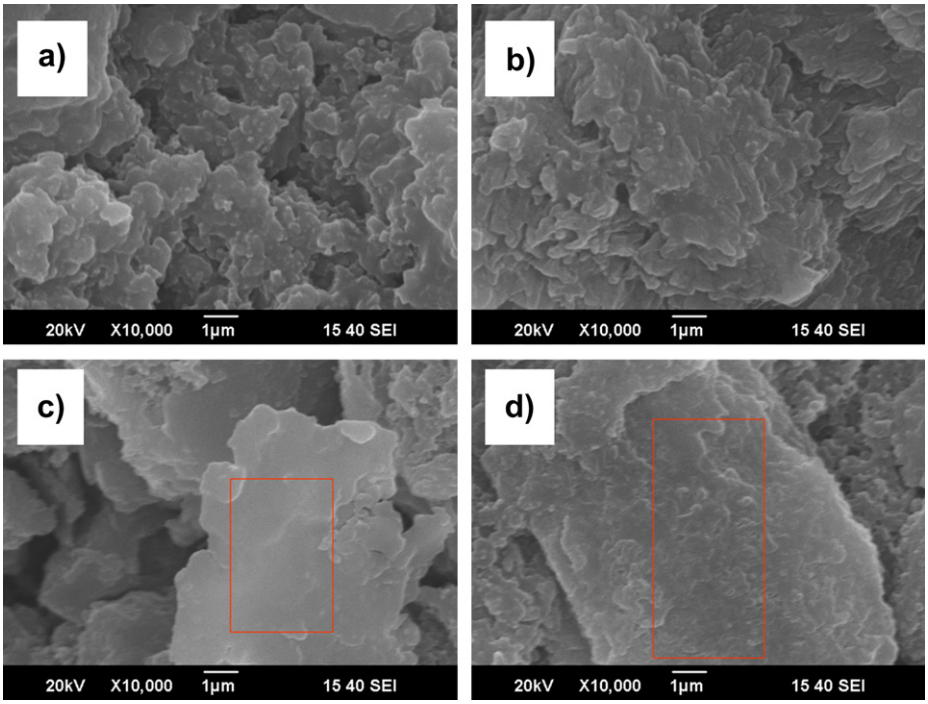

Fig. 11. SEM micrographs of different samples after 40 cycles: a) sticktight-like Co_3O_4 calcined at 400 °C; b) sticktight-like Co_3O_4 calcined at 500 °C; c) nanosheet Co_3O_4 calcined at 400 °C and d) nanosheet Co_3O_4 calcined at 500 °C.

the first several cycles even when the current density increases from 1 C to 2 C, due to the same reason as explained above for the cycling results. When the calcination temperature increases to 500 °C, the rate performance of the sticktight-like sample becomes worse because the capacity decreases fast with increasing the current density (Fig. 12b). However, the nanosheet sample also exhibits good rate performance that over 700 mAh g^{-1} can be retained at 10 C. The difference between these two samples is that the mechanical strength of the sticktight-like sample (1D) is weaker than that of the nanosheet sample (2D). After the powder mixing and grinding during the electrode preparation process, the sticktight-like particles are broken into smaller pieces (Fig. 7b). The smaller particle size may lead to the increase in the degree of side reactions between the Co_3O_4 particles and the electrolyte solution [28]. Consequently, the Co_3O_4 electrode of the nanosized particles experiences a significant capacity fade at high C rates.

4. Conclusions

Basic cobaltous carbonates with sticktight-like and nanosheet morphologies can be synthesized through a hydrothermal process at different temperatures. After calcinations at 400 °C and 500 °C, Co_3O_4 with the same morphologies can be obtained and used as electrode materials of lithium ion battery. Both the lower calcination temperature at 400 °C and the nanosheet morphology are beneficial to achieve better electrochemical performance. The electrochemical test shows that the nanosheet Co_3O_4 samples, especially when calcined at low temperature, exhibit improved cyclic performance and rate performance.

Acknowledgments

This study was supported by National Science Foundation of China (grant nos. 20971117 and 10979049) and Education Department of Anhui Province (grant no. KJ2009A142). We are also grateful to the Solar Energy Operation Plan of Academia Sinica.

References

[1] F.D. Wu, Y. Wang, J. Mater. Chem. 21 (2011) 6636.
[2] K.M. Nam, J.H. Shim, D.W. Han, H.S. Kwon, Y.M. Kang, Y. Li, H. Song, W.S. Seo, J.T. Park, Chem. Mater. 22 (2010) 4446.
[3] H.J. Zhang, H.H. Tao, Y. Jiang, Z. Jiao, M.H. Wu, B. Zhao, J. Power Sources 195 (2010) 2950.
[4] P. Zhang, Z.P. Guo, Y.D. Huang, D.Z. Jia, H.K. Liu, J. Power Sources 196 (2011) 6987.
[5] X.Y. Xue, S. Yuan, L.L. Xing, Z.H. Chen, B. He, Y.J. Chen, Chem. Commun. 47 (2011) 4718.
[6] Y.Q. Fan, H.B. Shao, J.M. Wang, L. Liu, J.Q. Zhang, Chem. Commun. 47 (2011) 3469.
[7] C.K. Chan, R.N. Patel, M.J. O'Connell, B.A. Korgel, Y. Cui, ACS Nano 20 (2010) 1680.
[8] X.W. Lou, D. Deng, J.Y. Lee, J. Feng, L.A. Archer, Adv. Mater. 20 (2008) 258.
[9] N. Du, H. Zhang, B. Chen, J. Wu, X. Ma, Z. Liu, Y. Zhang, D. Yang, X. Huang, J. Tu, Adv. Mater. 19 (2007) 4505.
[10] W.Y. Li, L.N. Xu, J. Chen, Adv. Funct. Mater. 15 (2005) 851.
[11] Y. Li, B. Tan, Y. Wu, Nano Lett. 8 (2008) 265.
[12] J. Jiang, J. Liu, R. Ding, X. Ji, Y. Hu, X. Li, A. Hu, F. Wu, Z. Zhu, X. Huang, J. Phys. Chem. C 114 (2010) 929.
[13] L. Tian, H. Zou, J. Fu, X. Yang, Y. Wang, H. Guo, X. Fu, C. Liang, M. Wu, P. Shen, Q. Gao, Adv. Funct. Mater. 20 (2010) 617.
[14] Y. Wang, H. Xia, L. Lu, J. Lin, ACS Nano 4 (2010) 1425.
[15] X.W. Lou, D. Deng, J.Y. Lee, L. Archer, J. Mater. Chem. 18 (2008) 4397.
[16] J.S. Do, R.F. Dai, J. Power Sources 189 (2009) 204.
[17] H.C. Liu, S.K. Yen, J. Power Sources 15 (2007) 478.
[18] Z.W. Fu, Y. Wang, Y. Zhang, Q.Z. Qin, Solid State Ion. 170 (2004) 105.
[19] Y. Sun, X.Y. Feng, C.H. Chen, J. Power Sources 196 (2011) 784.
[20] R. Xu, H.C. Zeng, J. Phys. Chem. B 107 (2003) 12643.
[21] H. Li, P. Balaya, J. Maier, J. Electrochem. Soc. 151 (2004) A1878.
[22] Y. Yu, C.H. Chen, J.L. Shui, S. Xie, Angew. Chem. Int. Ed. 44 (2005) 7085.
[23] S. Grugeon, S. Laruelle, L. Dupont, J.M. Tarascon, Solid State Sci. 5 (2003) 895.
[24] Y. Qi, N. Du, H. Zhang, X. Fan, Y. Yang, D. Yang, Nanoscale 4 (2012) 991.
[25] H.S. Lee, J. Choi, J. Jin, J. Chun, S.M. Lee, H.J. Kim, S.U. Son, Chem. Commun. 48 (2012) 94.
[26] S.L. Xiong, J.S. Chen, X.W. Lou, H.C. Zeng, Adv. Funct. Mater. 22 (2012) 861.
[27] W. Luo, X.L. Hu, Y.M. Sun, Y.H. Huang, J. Mater. Chem. 22 (2012) 8916.
[28] A. Ponrouch, M.R. Palacin, J. Power Sources 212 (2012) 233.